Article

Journal of
Nanoscience and Nanotechnology
Vol. 18, 8426–8436, 2018
www.aspbs.com/jnn

Different Crystal Form Titania Supported Ruthenium Nanoparticles for Liquid Phase Hydrodeoxygenation of Guaiacol

Wei Long, Yang Lv, Pingle Liu*, Fang Hao, Wei Xiong, Xie Li, Haishuai Cui, and He'an Luo

College of Chemical Engineering, Xiangtan University, Xiangtan 411105, People's Republic of China

Titania supported Ruthenium-based catalysts were prepared for liquid phase hydrodeoxygenation of guaiacol to cyclohexanol. The catalytic performance is affected by the different crystal forms of titania supports. Anatase and rutile titania supported catalyst 5%Ru/a-r-TiO_2 presents higher BET surface area, better dispersion of Ru particles with smaller particle size of 3–4 nm, more acidic centers, and more $Ru^{\delta+}$ located at the boundary between anatase titania and rutile titania. Hence, 5%Ru/a-r-TiO_2 gives the best catalytic performance of 95.33% conversion of guaiacol and 79.23% selectivity to cyclohexanol, other products mainly include cyclohexane, benzene, cyclohexanone and 1,2-cyclohexanediol. Based on the results of this work, the possible reaction path for guaiacol hydrodeoxygenation was proposed.

Keywords: Guaiacol, Interface, Hydrodeoxygenation, TiO_2, Ruthenium Nanoparticles.

1. INTRODUCTION

Clean and pollution-free energy is one hotspot of modern scientific research.[1] Biomass derived liquid fuels have the potential to provide a renewable, carbon-neutral energy source so as to offset the shortage of fossil energy.[2] Some interesting specific feedstocks have been investigated such as carbohydrate, triglycerides, glycerol, 5-hydroxymethylfurfural, cellulose, hemicellulose and pentose, lignin, and ligncellulose.[3–11] The catalytic conversion of biomass and derivatives over diverse catalysts can obtain different chemicals,[12–14] and the research is interesting and valuable to the industrial promotion.

Compared with some typical biomass energy such as glucose or pentose, lignin can not be obtained by hydrolysis or fermentation.[15] Pyrolysis is the traditional technology to produce lignin, but the purity of lignin is not ideal. Since lignin contains low concentration of sulfur, nitrogen and high concentration of oxygen (30–40 wt%), the hydrodeoxygenation appears as a potential route for further use of lignin.[16] Guaiacol is a typical representative of lignin which has two O-containing functional groups of phenolic and methoxy, and hydrodeoxygenation studies of guaiacol cause a wide range of concern.[17]

Guaiacol hydrodeoxygenation can be carried out in gas phase or liquid phase. The results of guaiacol hydrodeoxygenation in fixed bed tubular reactor are shown in Table I. Phenol and catechol were the major products when the sulfide was used as the catalyst or the catalyst was treated in H_2S. Benzene, toluene and xylene were the major products over Fe or Ni based catalysts. Also, the support had obviously influence on product distribution and catalytic activity.

Listed in Table II are the catalytic performances of liquid phase hydrodeoxygenation of guaiacol. Phenol and catechol were the major products over Mo based catalysts, and cyclohexane was the major product over Ni, Cu, Pd or Pt based catalysts.

Whether in liquid phase or gas phase hydrodeoxygenation of guaiacol, the reaction temperature was relatively higher. Some researchers tried to study guaiacol hydrodeoxygenation under mild conditions. Kim et al. has found that guaiacol hydrogenation over bimetallic RuRe/C catalyst can be carried out under 473 K and 2 MPa, the selectivity to cyclohexane was 57.0%.[38] He et al. proposed that Pt/TiO_2 catalyst can be used for highly effective hydrodeoxygenation of guaiacol in a fixed-bed reactor at 558 K and 4 MPa, the conversion of guaiacol was 70% and the selectivity to cyclohexane was

*Author to whom correspondence should be addressed.

1533-4880/2018/18/8426/011 doi:10.1166/jnn.2018.16392

Table I. The gas-phase hydrodeoxygenation of guaiacol.

Catalysts	Reaction conditions	Conv/%	Major product	Yield/%	Ref.
25.8 wt% $CoMo/Al_2O_3$	573 K, 4 MPa, 100 ppm of H_2S, LHSV = 1 h^{-1}, 12 h	85	Phenol	25.5	[18, 19]
8.6 wt % Ni_2P/SiO_2	573 K, 0.1 MPa, LHSV = 59 h^{-1}, 20.2 min	59	Methoxybenzene	22.4	[20]
5 wt% Pd/ Al_2O_3	573 K, 0.1 MPa, LHSV = 59 h^{-1}, 0.339 min	70	Catechol	70.0	[20]
22 wt% Fe/SiO_2	673 K, 0.1 MPa, LHSV = 1.5 h^{-1}, 150 min	74	BTX[a]	38.3	[21]
10 wt% Fe/AC	673 K, 0.1 MPa, LHSV = 0.6 h^{-1}, 150 min	82	Phenol	71.2	[22]
10 wt% NiCo/Al-MCM-41	673 K, 0.1 MPa, LHSV = 1.67 h^{-1}, 150 min	100	Phenol	40.0	[23]
15 wt% FeNi/HBeta	693 K, 0.1 MPa, LHSV = 1 h^{-1}, 180 min	100	BTX[a]	56.8	[24]
5 wt% NiPd/γ-Al_2O_3	723 K, 0.1 MPa, LHSV = 0.6 h^{-1}, 180 min	29	Phenol	18.4	[25]
7 wt% NiFe/CNTs	573 K, 3.0 MPa, WLHSV = 6.0 h^{-1}, 120 min	99	Cyclohexane	82.6	[26]

Note: [a]BTX is the mixture of benzene, toluene and xylene.

Table II. The liquid-phase hydrodeoxygenation of guaiacol.

Catalysts	Reaction conditions	Conv/%	Major product	Yield/%	Ref.
10 wt% MoN/GCA	573 K, 3 MPa, 2~8 h	72	phenol and catechol	33	[27]
10 wt % MoCoN/SBA-15	573 K, 5 MPa, 3 h	79	phenol and catechol	42	[28]
55.4 wt% Ni/SiO_2	593 K, 17 MPa, 1 h	77.5	cyclohexane	44.8	[29]
10 wt% $NiCu/ZrO_2$–SiO_2	573 K, 5 MPa, 8 h	100	cyclohexane	96	[30]
10 wt% ReS_2/C	573 K, 5 MPa, 3~4 h	100	phenol	80	[31]
10 wt% $NiCu/ZrO_2$–SiO_2	573 K, 3 MPa, 8 h	100	cyclohexane	96.8	[32]
3.7 wt% $CoMo/\gamma$-Al_2O_3	523 K, 5.5 MPa, sulfided by H_2S	90	phenol and catechol	32.2	[33]
5 wt% MoS_2/C	573 K, 5 MPa, 4 h	30	catechol	21.3	[34]
2 wt% Pd/32 wt% WO_x/γ-Al_2O_3	573 K, 7 MPa, 2.5 h	100	cyclohexane	88	[35]
15 wt% Ni/CNTm	573 K, 5 MPa, 2 h	100	cyclohexane	65	[36]
0.5 wt% Pt/HBeta	523 K, 0.4 MPa, 2 h	95	cyclohexane	43.2	[37]

75%.[39–40] Among Rh, Ru, Pd and Pt noble metal catalysts, Ru based catalyst showed better catalytic performance in guaiacol hydrodeoxygenation.[41] Also, the reaction mechanism of guaiacol hydrodeoxygenation over noble catalysts were investigated by *Ab initio* studies and density function theory.[42–44]

As a magical material, titania has already performed great success in the fields of photocatalysis, adsorption, dye degradation, antibacteria, electrochemisy and medical treatment. Its optical or catalytic properties can be changed distinctly as the inner structure of titania is adjusted. Therefore, different crystal forms of titania may effect the catalytic activity,[45] and this strange phenomenon is very interesting, which can be investigated by catalytic reaction.

In this work, titania supported Ruthenium nanoparticles catalysts were studied in guaiacol hydrodeoxygenation under mild conditions, it exhibited high conversion of guaiacol and high selectivity to cyclohexanol, and the influence of the crystal form of titania support was focused on.

2. EXPERIMENTAL DETAILS

2.1. Materials

Titania P25 was purchased from Germany Degussa Co., Ltd. Ruthenium trichloride hydrate ($RuCl_3 \cdot 3H_2O$) was purchased from Sinopharm Chemical Reagent Corporation Limited. Butyl titanate, diethylene glycol, tetrabutylammonium chloride, decahydronaphthalene and guaiacol were purchased from Shanghai Macklin biochemical Co., Ltd. Ethanol, Ammonia (30%), Nitric acid, Urea, Ammonium bicarbonate, ethylbenzene, acetone and Sodium chloride with analytical grade were purchased from Sinopharm Chemical Reagent Corporation Limited. H_2 (99.99%) was provided by Zhuzhou Diamond Gas Company.

2.2. Catalyst Preparation

Anatase TiO_2 supported Ru catalyst: Firstly, 5 mL butyl titanate, 5 mL diethylene glycol and 20 mL tetrabutylammonium chloride were putted together in a flask and stirred for 30 minutes. Then, the mixture was putted into the crystallization kettle and placed in a muffle stove at 473 K for 24 h. After being cooled to room temperature, the grey solid was washed for several times with distilled water in order to remove the ammonium ion and chloride ion. After washing with absolute ethanol for three times, the solid was dried in air overnight at 393 K, crushed and calcined at 573 K for 2 h in a muffle stove. The light grey powder of anatase TiO_2 was obtained.

Anatase TiO_2 supported Ru catalyst was prepared by the equal volume impregnation method. A certain amount of $RuCl_3 \cdot 3H_2O$ was dissolved in distilled water. Then, anatase TiO_2 powder was added into the mixture and stirred for 10 h. And the mixture was aged for 2 h in a microwave washer and dried in air overnight at 393 K for 4 h and crushed. Then it was reduced under a stream of pure H_2 (100 mL/min) at 673 K for 2 h. The prepared catalyst was labeled as x%Ru/a-TiO_2, and

$x\%$ was the mass percentage of Ruthenium metal in the catalyst.

Brookite TiO_2 supported Ru catalyst: Firstly, 7.8 mL butyl titanate was added into the ammonia with 1.1 g sodium chloride and stirred for 5 h. Then, the mixture was putted into a crystallization kettle and placed in a muffle stove at 453 K for 6 h. After being cooled to room temperature, the white solid was washed several times with distilled water in order to remove the sodium ion and chloride ion. Then, after washing with absolute ethanol for three times, the solid was dried in air overnight at 383 K, crushed and calcined at 623 K for 2 h in a muffle stove. The white powder of brookite TiO_2 was obtained.

Brookite TiO_2 supported Ru catalyst was prepared according to the above method for Ru/a-TiO_2, and the catalyst was named as $x\%$Ru/b-TiO_2, and $x\%$ was the mass percentage of Ruthenium metal in the catalyst.

Rutile TiO_2 supported Ru catalyst: Actually, anatase TiO_2 can be converted into rutile TiO_2 through roasting under high temperature. Anatase TiO_2 powder was putted into a tube furnace for heat treatment at 1073 K under a stream of pure N_2 (100 mL/min). After being cooled to room temperature, the white powder was washed several times with distilled water and absolute ethanol, dried in air overnight at 393 K. The white powder of rutile TiO_2 was obtained.

Rutile TiO_2 supported Ru catalyst was prepared according to the above method for Ru/a-TiO_2, and the catalyst was named as $x\%$Ru/r-TiO_2 where $x\%$ was the mass percentage of Ruthenium metal in the catalyst.

Titania P25 supported Ru catalyst: Titania P25 white powder contains anatase TiO_2 and rutile TiO_2, and the mass ratio is approximately 4:1. So the titania P25 powder was washed several times with distilled water, dried in air overnight at 383 K. The as-prepared sample was crushed after being cooled to room temperature.

Titania P25 supported Ru catalyst was prepared according to the above method for Ru/a-TiO_2, and the catalyst was labeled as $x\%$Ru/p-TiO_2 where $x\%$ was the mass percentage of Ruthenium metal in the catalyst.

Anatase TiO_2 and rutile TiO_2 (mass ratio of 1:1) supported Ru catalyst: 4.14 g of Urea was dissolved in 80 mL of distilled water in flask A, Then, nitric acid was added into the mixture and stirred for 1 h. 8 mL of butyl titanate was dissolved in 10 mL ethanol in flask B and stirred for 1 h. The molar ratio of urea and butyl titanate is 3:1. The mixture in flask B was dripped into flask A at the speed of 1.0 mL/min. Then, the mixture was stirred for 4 h and aged overnight to obtain the yellow homogeneous hydrosol. The mixture was evaporated at 373 K to obtain the yellow powder, and the powder was crushed, calcined at 573 K for 2 h in a muffle stove. This yellow powder contained anatase TiO_2 and rutile TiO_2, and the mass ratio was 1:1.

Anatase TiO_2 and rutile TiO_2 (mass ratio of 1:1) supported Ru catalyst was prepared according to the above method for Ru/a-TiO_2, the catalyst was labeled as $x\%$Ru/a-r-TiO_2, and $x\%$ was the mass percentage of Ruthenium metal in the catalyst.

Anatase TiO_2 and brookite TiO_2 (mass ratio of 1:1) supported Ru catalyst: 9.0 mL of butyl titanate was dissolved in 15 mL of ethanol in flask A and stirred for 1 h. 4 mL of ethanol, 1.8 mL of distilled water, 0.6 mL of nitric acid and 2 g of ammonium bicarbonate were mixed together in flask B and stirred for 1 h (the molar ratio of ammonium bicarbonate and butyl titanate was 2:1). The mixture in flask B was dripped into flask A at the speed of 1.0 mL/min. Then, the mixture was stirred for 4 h and aged overnight to yield a yellow homogeneous gel, and the as-prepared gel was dried in air overnight at 383 K, the obtained sample was crushed and calcined at 573 K for 2 h in a muffle stove. The obtained powder contained anatase TiO_2 and brookite TiO_2, and the mass ratio was 1:1.

Anatase TiO_2 and brookite TiO_2 (mass ratio of 1:1) supported Ru catalyst was prepared according to the above method for Ru/a-TiO_2, the catalyst was labeled as $x\%$Ru/a-b-TiO_2 where $x\%$ was the mass percentage of Ruthenium metal in the catalyst.

2.3. Catalyst Characterization

The specific surface area, pore volume and pore size distribution of the samples were obtained by the nitrogen adsorption–desorption on a Quantachrome NOVA-2200e automated gas sorption system. Specific surface areas and pore size distributions were calculated by Brunauer-Emmett-Teller (BET) and Barrett-Joyner-Halenda (BJH) methods.

Fourier transform infrared (FT-IR) spectra of the samples were recorded on a Nicolet 380 spectrometer. The spectra of the samples were acquired in the wave number range of 400–4000 cm^{-1}.

Ammonia gas chemisorption was measured with Quantachrome ChemBET 3000. The samples were previously reduced in hydrogen stream and cooled to ambient temperature under a nitrogen stream. The ammonia gas chemisorption was performed at 333 K, and the ammonia gas pulses (0.02 mL) were injected until the eluted areas of consecutive pulses became constant.

Powder X-ray diffraction (XRD) patterns were determined on a D/max 2500 TC diffractometer using Cu Kα radiation ($\lambda = 1.542$ Å). The tube voltage was 40 kV, the current was 30 mA, and the scan range was 5–90° with the scanning rate of $1° \cdot min^{-1}$.

The pyridine adsorbed FT-IR spectra of the samples were recorded on a Nicolet iS^{TM} 10 spectrometer. The samples were dried in a hot air oven for 1 h at 373 K prior to pyridine treatment for IR measurements. The samples (~50 mg each) were poured loosely into a sample cup. The loosely filled sample contacted with pyridine (~0.1 cm^3) directly. Then the sample cup was kept in a hot air oven at 393 K for 1 h to remove physisorbed pyridine. After

cooling, the IR spectrum was recorded in the spectral range between 1700 and 1300 cm^{-1} with 256 scans and at a resolution of 4 cm^{-1} using KBr background.

The morphologies of the samples were observed with scanning electron microscope (SEM) on a JEOL JSM-6610 LV scanning microscope operated at an accelerating voltage of 5 kV. The surface morphologies and particle sizes were observed with transmission electron microscopy (TEM), and the microstructures of the samples were observed with high-resolution TEM (HRTEM) on a TecnaiG220 ST electron microscope. The instrumental magnification ranged from 2×10^4 to 10×10^6. The samples were deposited on a copper grid and coated with a holey carbon film.

The X-ray photoelectron spectroscopic (XPS) spectrum was collected on a Perkin Elmer PHI5000C spectrometer with Mg Kα radiation ($hv = 1253.6$ eV) as the exicitation source.

2.4. Procedure for Catalytic Test

Catalytic test was carried out in a 15 mL Teflon-lined stainless steel autoclave with a magnetic stirrer at 400 rpm. Typically, 4.8 g of decahydronaphthalene, 1.2 g of guaiacol and 0.2 g of catalyst powder (200–400 μm) were added into the autoclave. The reactor was sealed and purged with H_2 to exclude air for five times, and then it was pressurized to 2.0 MPa with H_2 under vigorous stirring after the required temperature reached. After the reaction, the catalysts were separated by filtration from the liquid phase products. The contents of the reactants and the liquid phase products were determined with gas chromatography (Agilent Technologies, 7890 A) equipped with a DB-7501 capillary column (0.50 mm in diameter and 30 m in length) and a flame ionization detector (FID) using ethylbenzene as the internal standard. The liquid phase products include cyclohexane, benzene, cyclohexanol, cyclohexanone and phenol.

Carbon-based guaiacol conversion (w_{Gua}), product selectivity (S_i) was calculated according to the following equations.[46, 47] In this work, we can ignore the carbon proportion between the reactant and products because all the concerned products contain hexatomic ring, and i means the product i.

$$w_{Gua}\ (\%) = \frac{\mathrm{Mol(gua)_{in}} - \mathrm{Mol(gua)_{out}}}{\mathrm{Mol(gua)_{in}}} \times 100$$

$$S_i\ (\%) = \frac{\mathrm{Mol}_i}{\mathrm{Mol_{reacted \cdot Gua}}} \times 100$$

3. RESULTS AND DISCUSSION

3.1. Characterization of Catalysts

Shown in Figure 1 are three kinds of unit cell of TiO_2 based on the inorganic crystal database (ISCD, http://www.icsd.fiz-karlsruhe.de). Although the bond length between Ti atom and O atom is 0.195∼0.198 nm in TiO_2 with different crystal forms, the atomic arrangement of anatase TiO_2 is regular. The unit cell of brookite TiO_2 shows obviously oblique cubic feature, and the unit cell of rutile TiO_2 presents apparently octahedron feature.

Table III demonstrates textural properties of different catalysts with the same loading amount of Ru metal. It can be seen from Table III that the textural properties vary with the different crystal forms of titania. Anatase TiO_2 and rutile TiO_2 with mass ratio of 1:1 supported Ru catalyst 5%Ru/a-r-TiO_2 has the largest surface area and the smallest particle size. The average pore size is 7.5 nm and the pore volume is 0.23 $cm^3 \cdot g^{-1}$, which is at the intermediate level.

N_2 adsorption–desorption isotherms and pore size distributions of the samples are shown in Figures 2(a) and (b). According to the IUPAC classification, it can be seen that the hysteresis loop of 5%Ru/a-TiO_2 is of type H1, the pore diameter distribution is centered at 4.5 nm. The hystersis

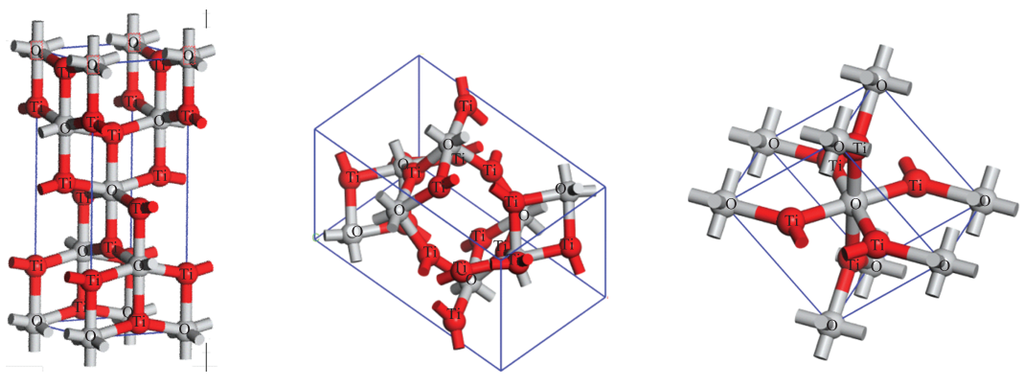

(a)anatase TiO_2
Unit cell:Ti_4O_8
0.38 nm×0.38 nm×0.95 nm

(b)brookite TiO_2
Unit cell:Ti_8O_{16}
0.92 nm×0.54 nm×0.51 nm

(c)rutile TiO_2
Unit cell:Ti_2O_4
0.46 nm×0.46 nm×0.30 nm

Figure 1. The unit cell structures of TiO_2.

Table III. Textural properties of catalysts.

Catalysts	Surface area ($m^2 \cdot g^{-1}$)	Average pore size (nm)	Pore volume ($cm^3 \cdot g^{-1}$)	Particle size[a] (nm)
5%Ru/a-TiO_2	58.3	4.3	0.09	82.9
5%Ru/b-TiO_2	63.4	29.6	0.44	94.7
5%Ru/r-TiO_2	14.5	11.7	0.04	414.6
5%Ru/p-TiO_2	50.8	32.8	0.42	118.2
5%Ru/a-r-TiO_2	93.7	7.5	0.23	64.0
5%Ru/a-b-TiO_2	88.2	7.3	0.17	68.0

Note: [a]Average diameter of particle size determined by the nitrogen adsorption–desorption.

loops of 5%Ru/b-TiO_2 and 5%Ru/r-TiO_2 are of type H4, which is associated with narrow slit-shaped pores. As shown in Figure 2(b), the hysteresis loops of 5%Ru/a-r-TiO_2 and 5%Ru/a-b-TiO_2 are of type H4 with highly ordered pores, and the pore diameter distribution are centered at 9.5 nm and 13.5 nm. It is shown that the mixture of different crystal form titania can form mesoporous materials.

The FT-IR spectra of the samples are shown in Figure 3. The bands around 1640 cm^{-1} in all the samples are attributed to the bending and stretching vibration peak of Ti–O. The band around of 3400 cm^{-1} in all the samples are attributed to the bending peak of active hydroxy on the surfaces of the catalysts. The broader the area of the band is, the more amount of the active hydroxy.

The TPR profiles of the samples are given in Figure 4. The TPR curves show that the initial reduction temperature of 5%Ru/r-TiO_2 is 537 K, which is higher than other samples. When the mixed crystal form of titania was used as the support, the initial reduction temperature is about 427 K or 455 K, it indicate that the mixed crystal form titania supported Ruthenium catalyst is more easier to be reduced.

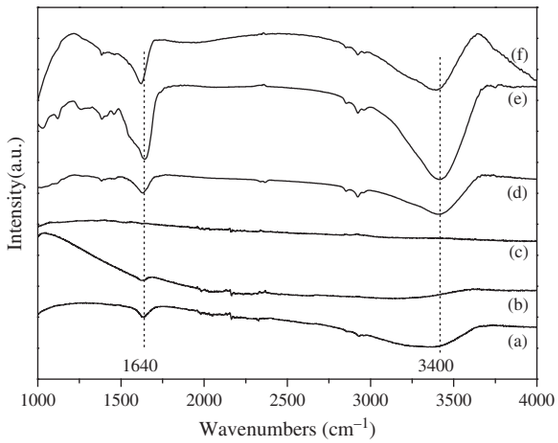

Figure 3. FT-IR spectra. (a) 5%Ru/a-TiO_2, (b) 5%Ru/b-TiO_2, (c) 5%Ru/r-TiO_2, (d) 5%Ru/p-TiO_2, (e) 5%Ru/a-r-TiO_2 and (f) 5%Ru/a-b-TiO_2.

The XRD spectra of the samples are shown in Figure 5, exhibiting the characteristic diffraction peaks of the titania with different crystal forms. The diffraction peaks of 5%Ru/a-TiO_2, 5%Ru/b-TiO_2 and 5%Ru/r-TiO_2 are accord with the diffractograms of anatase TiO_2 (JCPDS 21-1272), Brookite TiO_2 (JCPDS 29-1360) and rutile TiO_2 (JCPDS 21-1276).[48] As to the titania support with mixed crystal forms, the simple formula of $A_R/(A_A + A_R)$ is used to judge the crystal form proportion, where A_A and A_R represent the integrated intensities of the (101) peak of anatase and the strongest (110) peak of rutile respectively.[49, 50] Hence, the mass proportion of the different crystal form titania in 5%Ru/p-TiO_2, 5%Ru/a-r-TiO_2 and 5%Ru%/a-b-TiO_2 can be estimated. Obviously, the characteristic diffraction peak at $2\theta = 44°$ is ascribed to the (101) crystalline plane of Ru (JCPDS 88-1734). The diffraction peak of Ru(101) in mixed crystal form titania supported catalyst is weaker than that of single crystal form titania supported catalyst of

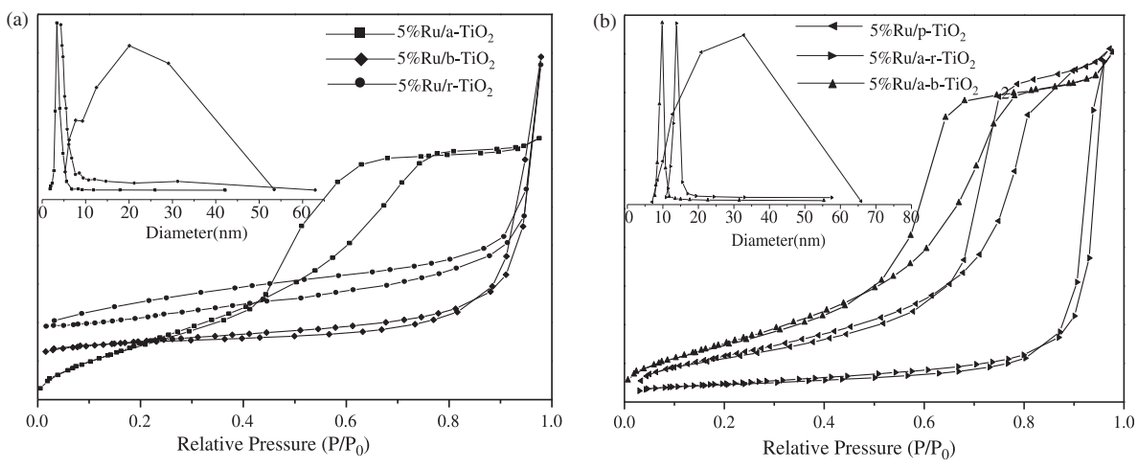

Figure 2. N_2 adsorption–desorption isotherms and pore size distributions. (a) 5%Ru/a-TiO_2, 5%Ru/b-TiO_2 and 5%Ru/r-TiO_2; (b) 5%Ru/p-TiO_2, 5%Ru/a-r-TiO_2 and 5%Ru/a-b-TiO_2.

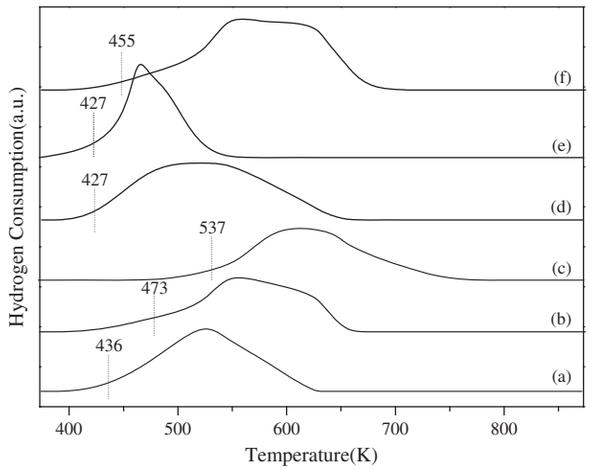

Figure 4. H_2-TPR profiles of some catalysts. (a) 5%Ru/a-TiO_2, (b) 5%Ru/b-TiO_2, (c) 5%Ru/r-TiO_2, (d) 5%Ru/p-TiO_2, (e) 5%Ru/a-r-TiO_2 and (f) 5%Ru/a-b-TiO_2.

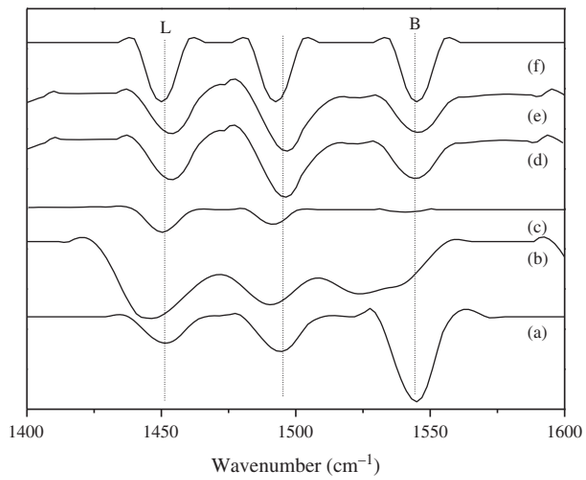

Figure 6. Pyridine adsorbed FT-IR spectra of some catalysts. (a) 5%Ru/a-TiO_2, (b) 5%Ru/b-TiO_2, (c) 5%Ru/r-TiO_2, (d) 5%Ru/p-TiO_2, (e) 5%Ru/a-r-TiO_2 and (f) 5%Ru/a-b-TiO_2.

5%Ru/a-TiO_2, 5%Ru/b-TiO_2 and 5%Ru/r-TiO_2. The mixed crystal form titania is in favour of Ru dispersion, and Ru particles in 5%Ru/a-r-TiO_2 show better dispersion.

The pyridine adsorbed FT-IR spectra of the samples are shown in Figure 6. The IR band at 1450 cm^{-1} is the adsorption peak of pyridine on Lewis acidic centers, the band at 1490 cm^{-1} corresponds to the interaction of pyridine with Lewis and Brønsted acid sites, and the band at 1540 cm^{-1} is perceived as the adsorption peak of pyridine on Brønsted acid centers. The results of the pyridine FT-IR spectra indicate that the Brønsted acid centers predominate in the anatase titania support while brookite titania support possesses more Lewis acidic centers, and the acidic center decreases when 5%Ru/r-TiO_2 was calcined at higher temperature. Both the Lewis acidic centers and the Brønsted acid sites exist in the mixed crystal form titania supported catalysts of 5%Ru/p-TiO_2, 5%Ru/a-r-TiO_2 and 5%Ru/a-b-TiO_2, the different acidic center may have influence on the catalytic performance.

The NH_3-TPD results of the samples are given in Figure 7. Compared with the mixed crystal form titania supported catalysts, the single crystal form titania supported catalysts presents cuspidal NH_3 desorption peak and possesses relatively less acidic centers.

The scanning electron microscope (SEM) images of the samples are shown in Figure 8. 5%Ru/a-TiO_2 and 5%Ru/b-TiO_2 show obvious lump and flake structure, and 5%Ru/r-TiO_2 calcined at higher temperature presents coral structure. It can be seen form Figures 8(d)–(f) that 5%Ru/p-TiO_2 particles conglomerate, but there are no obvious conglomeration in 5%Ru/a-r-TiO_2 and

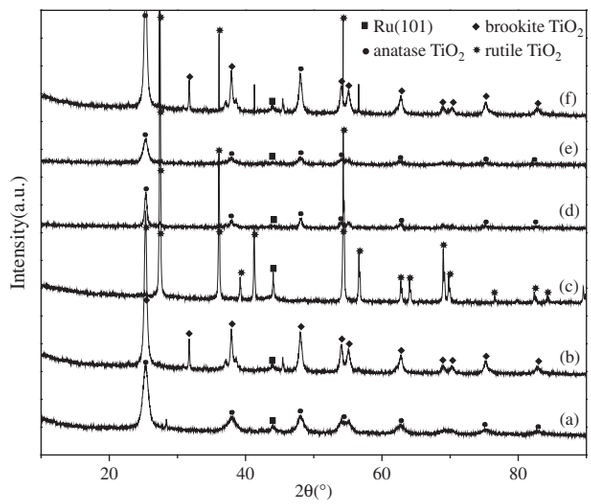

Figure 5. X-ray diffraction (XRD) patterns of some catalysts. (a) 5%Ru/a-TiO_2, (b) 5%Ru/b-TiO_2, (c) 5%Ru/r-TiO_2, (d) 5%Ru/p-TiO_2, (e) 5%Ru/a-r-TiO_2 and (f) 5%Ru/a-b-TiO_2.

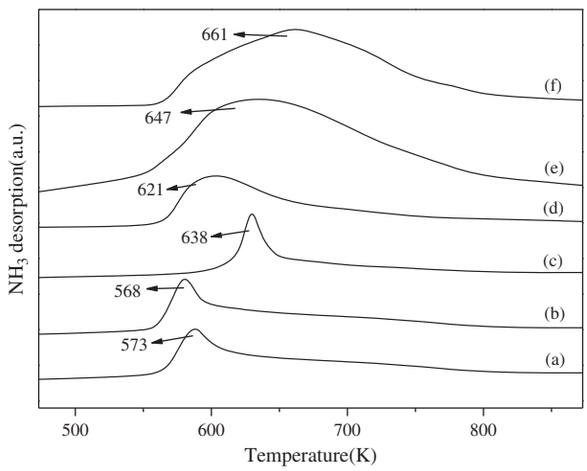

Figure 7. NH_3-TPD of some catalysts. (a) 5%Ru/a-TiO_2, (b) 5%Ru/b-TiO_2, (c) 5%Ru/r-TiO_2, (d) 5%Ru/p-TiO_2, (e) 5%Ru/a-r-TiO_2 and (f) 5%Ru/a-b-TiO_2.

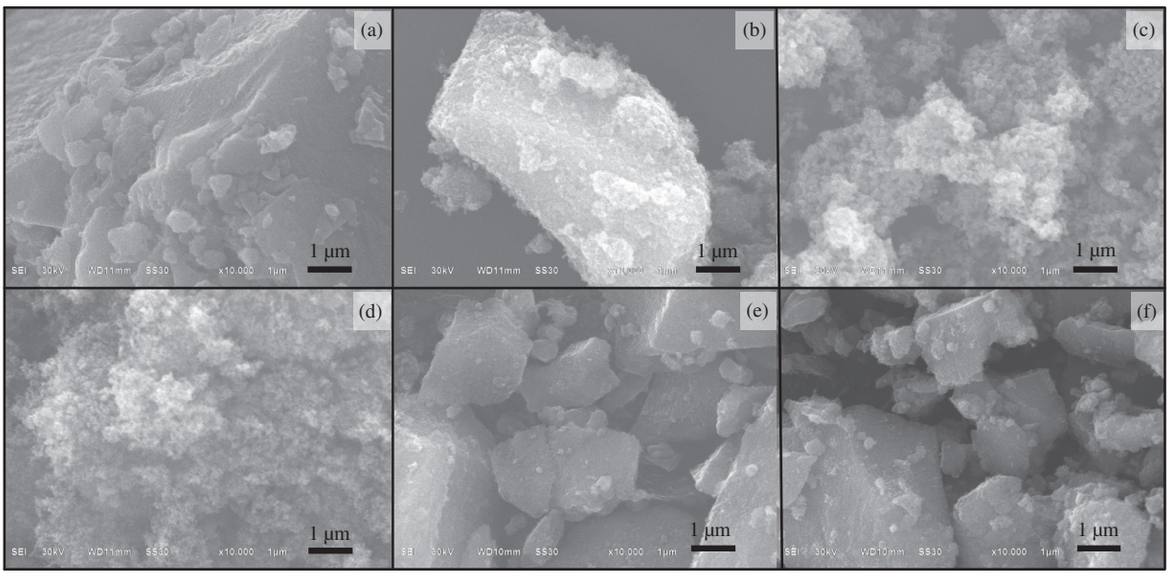

Figure 8. The SEM images. (a) 5%Ru/a-TiO_2, (b) 5%Ru/b-TiO_2, (c) 5%Ru/r-TiO_2, (d) 5%Ru/p-TiO_2, (e) 5%Ru/a-r-TiO_2 and (f) 5%Ru/a-b-TiO_2.

5%Ru/a-b-TiO_2. The proportion of different crystal form of titania support has influence on its morphological structure.

The TEM images of 5%Ru/a-r-TiO_2 are shown in Figure 9. It can be seen from Figure 9 that Ru particles are shown better dispersion and are centered at 3–4 nm. The crystal lattices of anatase titania and rutile titania are shown in Figure 9, and there exists clear intersectant lattice. It is worth mentioned that some Ru particles are located at the boundary between anatase titania and rutile titania, which are defined as $Ru^{\delta+}$ and may show different properties.[49,50] The particle size distribution of 5%Ru/a-r-TiO_2 is shown in Figure 10, and the Ru particle sizes centered at 3–4 nm.

The X-ray photoelectron spectroscopic (XPS) spectra are shown in Figure 11. The spectra are deconvolved to resolve the respective contributions because the peaks of Ti2*p* partly overlap with the peaks of Ru3$p_{3/2}$. A comparison of the XPS spectra of Figures 11(a) and (b) reveals that there is not any peak of $Ru^{\delta+}$ in 5%Ru/a-b-TiO_2 (Fig. 11(b)) while the peaks around 485.5 and 463.7 eV in 5%Ru/a-r-TiO_2 (Fig. 11(a)) are attributed to $Ru^{\delta+}3p_{1/2}$

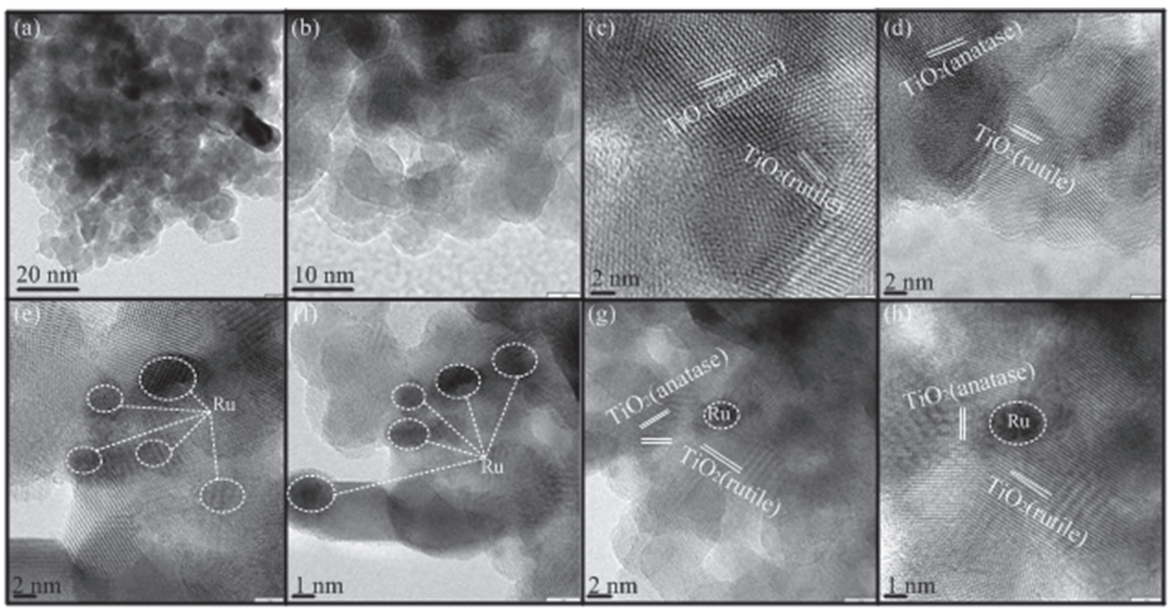

Figure 9. TEM images of 5%Ru/a-r-TiO_2 catalyst.

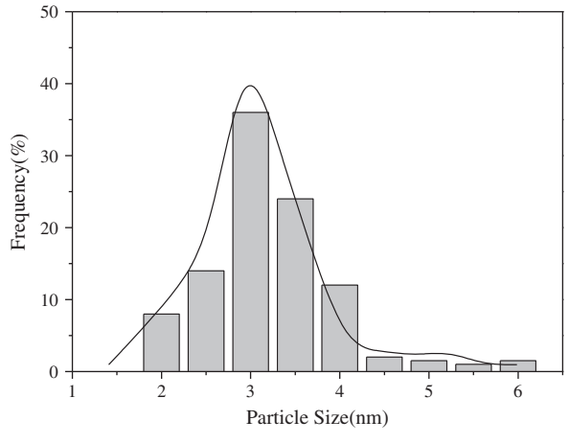

Figure 10. Particle size distribution of 5%Ru/a-r-TiO_2 catalyst.

and $Ru^{\delta+}3p_{3/2}$. Moreover, the titania satellite peak exists both in 5%/a-b-TiO_2 and 5%Ru/a-r-TiO_2.[51, 52]

The fitting results with regard to Ru are displayed in Table IV. The peak around 483.3 eV is attributed to the $Ru^0 3p_{1/2}$ spectral peak and the peak around 461.1 eV is ascribed to the $Ru^0 3p_{3/2}$ spectral peak. There are only $Ru^0 3p_{1/2}$ and $Ru^0 3p_{3/2}$ peaks in 5%Ru/a-b-TiO_2. However, besides $Ru^0 3p_{1/2}$ and $Ru^0 3p_{3/2}$ peaks, there are $Ru^{\delta+}3p_{1/2}$ and $Ru^{\delta+}3p_{3/2}$ peaks around 485.5 and 463.7 eV in 5%Ru/a-r-TiO_2, and the integral percentages are 6.1% and 6.9%, respectively.

3.2. Catalytic Performance

Figure 12 shows the guaiacol conversion and product selectivity over Ru supported on different crystal form titania, the effects of the loading amount of Ru between 3 wt.% to 6 wt.% are tested. By comparing the catalytic performance over Ru supported catalysts, one can find that the catalytic performance is affected by the different

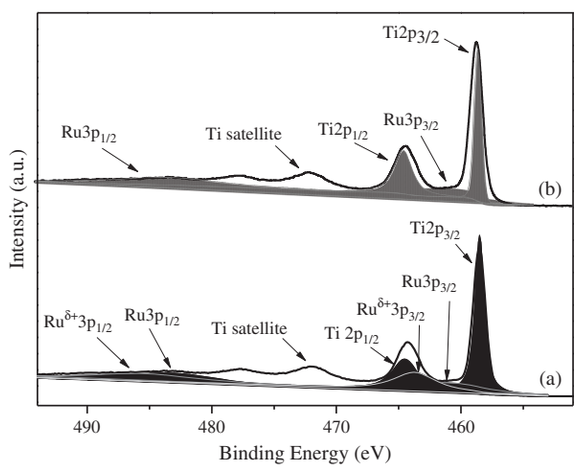

Figure 11. The Ru3*p* and Ti2*p* spectra of (a) 5%Ru/a-r-TiO_2 and (b) 5%Ru/a-b-TiO_2.

Table IV. The deconvolution results of the Ru3*p* spectra.

Catalyst	Peak	Peak position (eV)	FWHM (eV)[a]	Integral percentage (%)[b]
5%Ru/a-r-TiO_2	$Ru^0\ 3p_{1/2}$	483.3	2.83	30.7
	$Ru^0\ 3p_{3/2}$	461.1	2.87	56.3
	$Ru^{\delta+}\ 3p_{1/2}$	485.5	2.94	6.1
	$Ru^{\delta+}\ 3p_{3/2}$	463.7	2.96	6.9
5%Ru/a-b-TiO_2	$Ru^0\ 3p_{1/2}$	483.3	3.12	34.6
	$Ru^0\ 3p_{3/2}$	461.1	3.11	65.4

Notes: [a]The full width at half maximum of the peak. [b]The percentage of the integral of each peak to the sum of the integrals of all the fitted Ru peaks.

crystal form titania and the guaiacol conversion increases with the increment of the loading amount of Ru. When the loading amount of Ru metal is greater than 5 wt.%, the selectivity to cyclohexanol shows a decreasing trend because more cyclohexanol can be transformed to cyclohexane under such condition. Hence, the suitable loading amount of Ru metal is 5 wt.%.

In general, mixed crystal form titania supported catalysts show better catalytic performance than that of single crystalline titania supported catalysts, moreover, it can be seen from Table V that 5%Ru/a-r-TiO_2 gives the best catalytic performance of 95.33% conversion of guaiacol and 79.23% selectivity to cyclohexanol. Compared with other catalysts, 5%Ru/a-r-TiO_2 presents higher BET surface area, better dispersion of Ru particles with smaller particle size of 3–4 nm, more acidic centers, and more $Ru^{\delta+}$ located at the boundary between anatase titania and rutile titania.

Besides cyclohexanol, the products of guaiacol hydrodeoxygenation include cyclohexane, benzene, cyclohexanone, phenol and 1,2-cyclohexanediol. Curve (h) in Figure 12 refers to the selectivity to the products of others, including anisole, catechol, toluene, xylene, dimethoxybenzene, methlguaiacol and methoxy cyclohexanol.

Effect of the reaction time on the hydrodeoxygenation of guaiacol is shown in Figure 13. It can be seen that the conversion of guaiacol gradually increases with the prolonged reaction time, while the selectivity to cyclohexanol increases when the reaction time is less than 3 hours and decrease apparently after 3 h. Hence, the suitable reaction time for guaiacol hydrodeoxygenation over 5%Ru/a-r-TiO_2 catalyst under 473 K and 2.0 MPa is 3 h.

3.3. The Possible Reaction Path

On the basis of the results in this work and some literatures,[48, 49] the possible reaction path for guaiacol hydrodeoxygenation over 5%Ru/TiO_2 was shown in Scheme 1. Guaiacol hydrodeoxygenation is a complex process, cyclohexanol and cyclohexane can be obtained in this reaction. There exist some routes to the product of cyclohexanol, and cyclohexane is the product of the excess hydrogenolysis process.

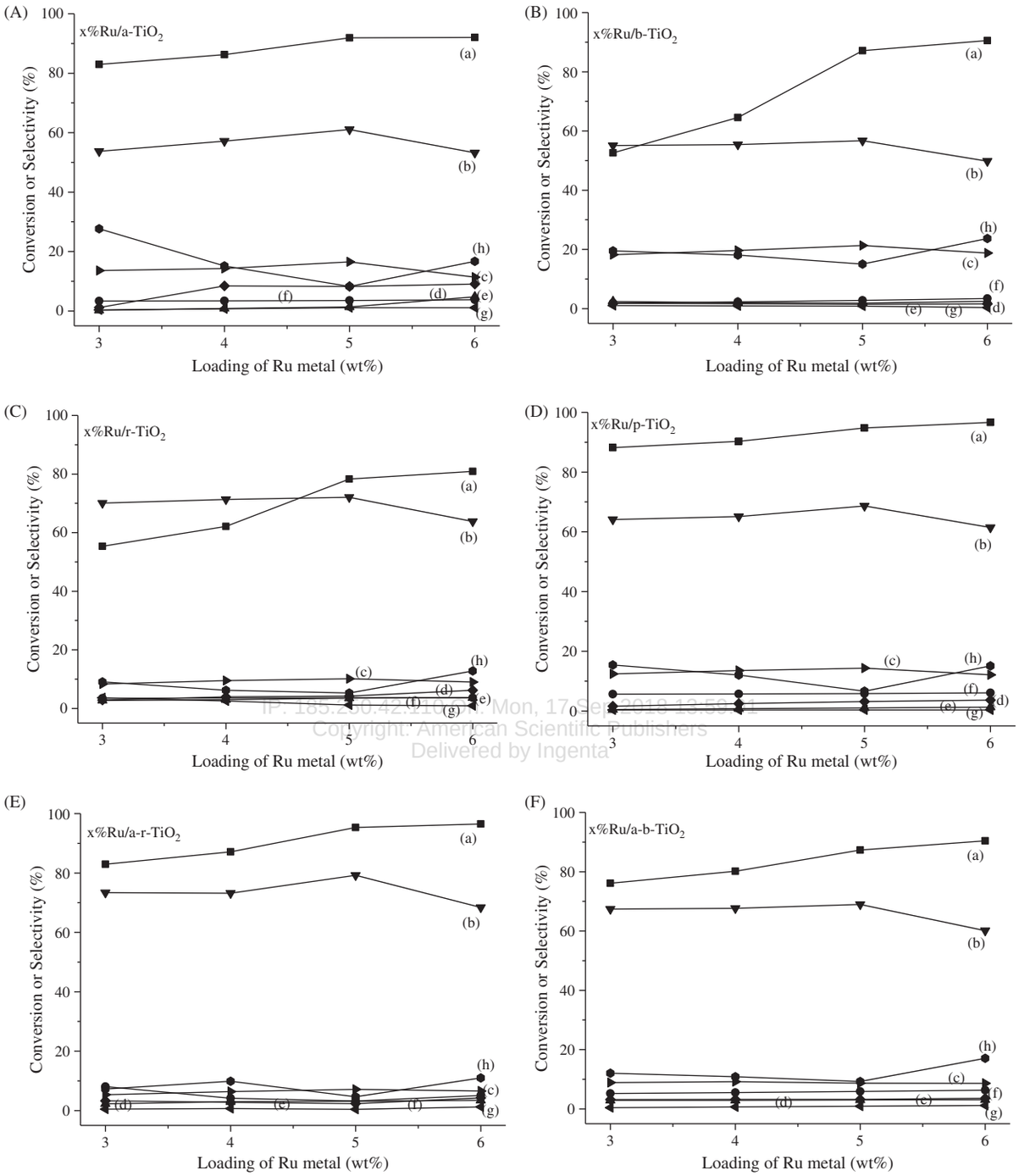

Figure 12. The catalytic performance under the loading amount of Ru metal. (A) *x*%Ru/a-TiO_2, (B) *x*%Ru/b-TiO_2, (C) *x*%Ru/r-TiO_2, (D) *x*%Ru/p-TiO_2, (E) *x*%Ru/a-r-TiO_2, and (F) *x*%Ru/a-b-TiO_2. (a) conversion, (b) cyclohexanol, (c) 1,2-cyclohexanediol, (d) cyclohexanone, (e) benzene, (f) cyclohexane, (g) phenol, (h) others. Reaction conditions: 0.2 g of catalyst, temperature 473 K, H_2 pressure 2.0 MPa, stirring rate 400 rpm and time 3 h.

In this work, we have found that benzene hydrogenation in guaiacol hydrodeoxygenation prefers to take place and demethylation process inevitably occurs in this reaction, this is also in accordance with the literatures.[46, 53, 54] It can be seen from Scheme 1 that guaiacol can be hydrogenated to phenol, catechol, 2-methoxy cyclohexanol and 2-methoxycyclohexanone which have been testified by GC-MS, and these intermediates can be further transformed to cyclohexanol and cyclohexane.

Table V. Results of guaiacol hydrodeoxygenation.

Catalyst	w_{Gua} (%)	S_i(%)						
		Cyclohexane	Benzene	Cyclohexanol	Cyclohexanone	Phenol	1,2-cyclohexanediol	Others[a]
5%Ru/a-TiO_2	91.89	3.52	1.32	61.09	8.23	1.08	16.54	8.22
5%Ru/b-TiO_2	87.13	2.76	1.87	56.73	1.44	0.82	21.33	15.05
5%Ru/r-TiO_2	55.33	3.43	2.70	70.05	2.83	3.62	8.32	9.05
5%Ru/p-TiO_2	94.78	5.82	1.04	68.66	3.17	0.37	14.33	6.61
5%Ru/a-r-TiO_2	95.33	3.10	3.12	79.23	2.31	0.41	7.10	4.73
5%Ru/a-b-TiO_2	87.32	5.87	3.04	68.97	3.24	0.92	8.70	9.26

Notes: [a]The others contain: anisole, catechol, toluene, xylene, dimethoxybenzene, methlguaiacol and methoxy cyclohexanol. Reaction conditions: 0.2 g of catalyst, temperature 473 K, H_2 pressure 2.0 MPa, stirring rate 400 rpm and time 3 h.

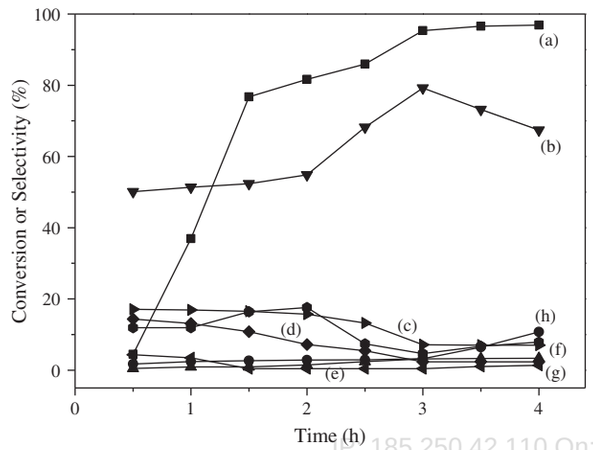

Figure 13. Effects of the reaction time over 5%Ru/a-r-TiO_2 catalyst. (a) conversion, (b) cyclohexanol, (c) 1,2-cyclohexanediol, (d) cyclohexanone, (e) benzene, (f) cyclohexane, (g) phenol, (h) others. Reaction conditions: 0.2 g of catalyst, temperature 473 K, H_2 pressure 2.0 MPa, stirring rate 400 rpm.

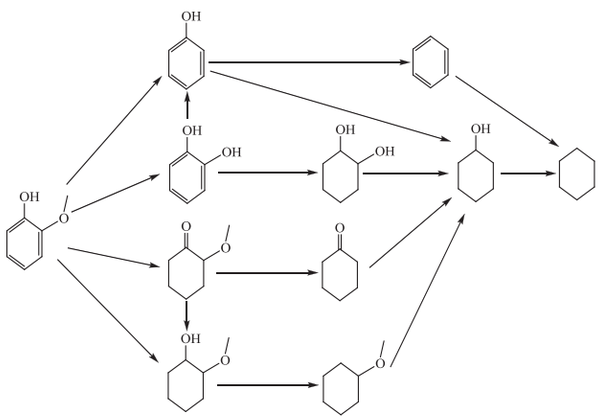

Scheme 1. Possible reaction path of guaiacol hydrodeoxygenation.

4. CONCLUSIONS

In conclusion, Ruthenium-based catalysts supported with titania possessing different crystal forms were prepared for liquid phase hydrodeoxygenation of guaiacol to cyclohexanol. The physicochemical properties of the prepared catalysts were characterized by FTIR, XRD, NH_3-TPD, SEM, HRTEM and XPS. The results showed that the catalytic performance was affected by the different crystal form titania support, and 5%-Ru/a-r-TiO_2 presented higher BET surface area, better dispersion of Ru particles with smaller particle size of 3–4 nm, more acidic centers, and more $Ru^{\delta+}$ located at the boundary between anatase titania and rutile titania. Hence, it was found that 5%Ru/a-r-TiO_2 gave the best catalytic performance of 95.33% conversion of guaiacol and 79.23% selectivity to cyclohexanol, other products mainly included cyclohexane, benzene, cyclohexanone and 1,2-cyclohexanediol. Finally, a possible reaction path for guaiacol hydrodeoxygenation was proposed based on this work and some literatures.

Acknowledgment: This work was supported by NSFC (U1662127), Project of Hunan province Science and Technology Department (2015GK1060) and Project of Education Department of Hunan Province (17A209), and Collaborative Innovation Center of New Chemical Technologies for Environmental Benignity and Efficient Resource Utilization.

References and Notes

1. M. Besson, P. Gallezot, and C. Pinel, *Chem. Rev.* 114, 1827 (**2013**).
2. T. P. Vispute, H. Y. Zhang, A. Sanna, R. Xiao, and G. W. Huber, *Science* 330, 1222 (**2010**).
3. M. J. Climent, A. Corma, and S. Iborra, *Green Chem.* 13, 520 (**2011**).
4. A. Behr and J. P. Gomes, *Eur. J. Lipid. Sci. Tech.* 112, 31 (**2010**).
5. B. Katryniok, H. Kimura, E. Skrzyńska, J. S. Girardon, P. Fongarland, M. Capron, R. Ducoulombier, N. Mimura, S. Paul, and F. Dumeiqnil, *Green Chem.* 13, 1960 (**2011**).
6. R. J. van Putten, J. C van der Waal, E. D. De Jong, C. B. Resrendra, H. J. Heeres, and J. G. de Vries, *Chem. Rev.* 113, 1499 (**2013**).
7. H. Kobayashi, H. Ohta, and A. Fukuoka, *Catal. Sci. Technol.* 2, 869 (**2012**).
8. T. Gan, Z. X. Shi, K. L. Wang, J. Y. Sun, Z. Lv, and Y. M. Liu, *Aust. J. Chem.* 69, 220 (**2015**).
9. M. P. Pandey and C. S. Kim, *Chem. Eng. Technol.* 34, 29 (**2011**).
10. G. Centi, P. Lanzafame, and S. Perathoner, *Catal. Today* 167, 14 (**2011**).
11. C. H. Zhou, X. Xia, C. X. Lin, and J. Beltramini, *Chem. Soc. Rev.* 40, 5588 (**2011**).
12. M. J. Climent, A. Corma, and S. Iborra, *Green Chem.* 16, 516 (**2014**).
13. A. Kruse, A. Funke, and M. M. Titirici, *Curr. Opin. Chem. Biol.* 17, 515 (**2013**).

14. T. Ennaert, J. Van Aelst, J. Dijkmans, R. D. Clercq, W. Schutyser, M. Dusselier, D. Verboekend, and B. F. Sels, *Chem. Soc. Rev.* 45, 584 (**2016**).
15. A. Jain, R. Balasubramanian, and M. P. Srinivasan, *Chem. Eng. J.* 283, 789 (**2016**).
16. C. Li, X. Zhao, A. Wang, G. W. Huber, and T. Zhang, *Chem. Rev.* 115, 11559 (**2015**).
17. D. Gao, C. Schweitzer, H. T. Hwang, and A. Varma, *Ind. Eng. Chem. Res.* 53, 18658 (**2014**).
18. V. N. Bui, G. Toussaint, D. Laurenti, C. Mirodatos, and C. Geantet, *Catal. Today* 143, 172 (**2009**).
19. V. N. Bui, D. Laurenti, P. Afanasiev, and C. Geantet, *Appl. Catal. B-Environ.* 101, 239 (**2011**).
20. H. Y. Zhao, D. Li, P. Bui, and S. T. Oyama, *Appl. Catal. A-Gen.* 391, 305 (**2012**).
21. R. N. Olcese, M. Bettahar, D. Petitjean, B. Malaman, and F. Giovanella, *Appl. Catal. B-Environ.* 115, 63 (**2012**).
22. R. Olcese, M. M. Bettahar, B. Malaman, J. Ghanbaja, L. Tibavizco, D. Petitjean, and A. Dufour, *Appl. Catal. B-Environ.* 129, 528 (**2013**).
23. N. T. T. Tran, Y. Uemura, S. Chowdhury, and A. Ramli, *Appl. Catal. A-Gen.* 512, 93 (**2016**).
24. X. Xu, E. Jiang, Y. Du, and B. Li, *Renew. Energ.* 96, 458 (**2016**).
25. Q. Lai, C. Zhang, and J. H. Holles. *Appl. Catal. A-Gen.* 528, 1 (**2016**).
26. H. Fang, J. Zheng, X. Luo, J. Du, A. Roldan, S. Leoni, and Y. Yuan, *Appl. Catal. A-Gen.* 529, 20 (**2017**).
27. I. T. Ghampson, C. Sepúlveda, R. Garcia, L. R. Radovic, J. G. Fierro, W. J. DeSisto, and N. Escaona, *Appl. Catal. A-Gen.* 439, 111 (**2012**).
28. I. T. Ghampson, C. Sepúlveda, R. Garcia, J. G. Fierro, N. Escalona, and W. J. DeSisto, *Appl. Catal. A-Gen.* 435, 51 (**2012**).
29. M. V. Bykova, D. Y. Ermakov, V. V. Kaichev, O. A. Bulavchenko, A. A. Saraev, M. Y. Lebedev, and V. A. Yakovlev, *Appl. Catal. B-Environ.* 113, 296 (**2012**).
30. X. Zhang, T. Wang, L. Ma, Q. Zhang, Y. Yu, and Q. Liu, *Catal. Commun.* 33, 15 (**2013**).
31. C. Sepúlveda, R. García, P. Reyes, I. T. Ghampson, J. L. G. Fierro, D. Laurenti, M. Vrinat, and N. Escalona, *Appl. Catal. A-Gen.* 475, 427 (**2014**).
32. X. Zhang, Q. Zhang, L. Chen, Y. Xu, T. Wang, and L. Ma, *Chinese J. Catal.* 35, 302 (**2014**).
33. I. D. Mora, E. Méndez, L. J. Duarte, and S. A. Giraldo, *Appl. Catal. A-Gen.* 474, 59 (**2014**).
34. P. E. Ruiz, B. G. Frederick, W. J. De Sisto, R. N. Austin, L. R. Radovic, K. Leiva, R. Garcia, N. Escalona, and M. C. Wheeler, *Catal. Comm.* 27, 44 (**2012**).
35. Y. K. Hong, D. W. Lee, H. J. Eom, and K. Y. Lee, *Appl. Catal. B-Environ.* 150, 438 (**2014**).
36. A. B. Dongil, L. Pastor-Pérez, A. Sepúlveda-Escribano, R. Garcia, and N. Escalona, *Fuel* 172, 65 (**2016**).
37. E. H. Lee, R. Park, H. Kim, H. P. Sung, S. C. Jung, J. K. Jeon, S. C. Kim, and Y. K. Park, *J. Ind. Eng. Chem.* 37, 18 (**2016**).
38. M. Kim, J. M. Ha, K. Y. Lee, and J. Jae, *Catal. Commun.* 86, 113 (**2016**).
39. Z. He and X. Wang, *Front. Chem. Sci. Eng.* 8, 369 (**2014**).
40. Z. He, M. Hu, and X. Wang, *Catal. Today* 302, 136 (**2018**).
41. A. Gutierrez, R. K. Kaila, M. L. Honkela, R. Slioor, and A. O. I. Krause, *Catal. Today* 147, 239 (**2009**).
42. C. Agache and V. I. Popa, *Monatsh. Chem.* 137, 55 (**2006**).
43. C. Liu, Y. Zhang, and X. Huang, *Fuel Process. Technol.* 123, 159 (**2014**).
44. J. Lu and A. Heyden, *J. Catal.* 321, 39 (**2015**).
45. F. Han, X. Mao, and Q. H. Xu, *Sci. China. Chem.* 60, 521 (**2017**).
46. J. Sun, A. M. Karim, H. Zhang, L. Kovarik, X. H. S. Li, A. Hensley, J. S. McEwen, and Y. Wang, *J. Catal.* 306, 47 (**2013**).
47. X. Zhu, L. L. Lobban, R. G. Mallinson, and D. E. Resasco, *J. Catal.* 281, 21 (**2011**).
48. S. Boonyasuwat, T. Omotoso, D. E. Resasco, and S. P. Crossley, *Catal. Lett.* 143, 783 (**2013**).
49. G. B. Zhou, R. F. Dou, H. Z. Bi, S. H. Xie, Y. Per, K. N. Fan, M. H. Qiao, B. Sun, and B. N. Zong, *J. Catal.* 332, 119 (**2015**).
50. H. Zhang and J. F. Banfield, *J. Phys. Chem. B* 104, 3481 (**2000**).
51. M. Zahmkiran, Y. Tonbul, and S. ÖZkar, *J. Am. Chem. Soc.* 132, 6541 (**2010**).
52. J. Y. Shen, A. Adnot, and S. Kaliaguine, *Appl. Surf. Sci.* 51, 47 (**1991**).
53. M. Hellinger, H. W. P. Carvalho, S. Baier, D. Wang, W. Kleist, and J. D. Grunwaldt, *Appl. Catal. A-Gen.* 490, 181 (**2015**).
54. A. Aqsha, L. Katta, and N. Mahinpey, *Catal. Lett.* 145, 1351 (**2015**).

Received: 30 January 2018. Accepted: 26 March 2018.